

Raman scattering from optical phonons and magnetic excitations in $\text{Cd}_{1-x}\text{Mn}_x\text{Se}$ and $\text{Cd}_{1-x}\text{Mn}_x\text{S}$

E.-K. Suh,* Akhilesh K. Arora,[†] A. K. Ramdas, and S. Rodriguez

Department of Physics, Purdue University, West Lafayette, Indiana

(Received 21 May 1991; revised manuscript received 7 October 1991)

The Raman spectra of $\text{Cd}_{1-x}\text{Mn}_x\text{Se}$ and $\text{Cd}_{1-x}\text{Mn}_x\text{S}$ are investigated for various Mn^{2+} concentrations x . Both $\text{Cd}_{1-x}\text{Mn}_x\text{Se}$ and $\text{Cd}_{1-x}\text{Mn}_x\text{S}$ have the wurtzite structure and have point-group symmetry C_{6v} . $\text{Cd}_{1-x}\text{Mn}_x\text{Se}$ shows a two-mode behavior, whereas $\text{Cd}_{1-x}\text{Mn}_x\text{S}$, in which the modes associated with Mn^{2+} appear in between the LO and TO phonons, shows an intermediate behavior. The frequencies of the TO modes and nonpolar E_2 modes are found not to depend significantly on the composition. We believe that this is due to the absence of polarization fields associated with this mode. The modified random-element-isodisplacement model gives a good description of optical phonons in $\text{Cd}_{1-x}\text{Mn}_x\text{Se}$. In an external magnetic field, a Raman line associated with a spin-flip excitation of Mn^{2+} and its combination with LO phonons are observed.

I. INTRODUCTION

The tetrahedrally coordinated II-VI compound semiconductors in which a fraction of cation is replaced by a magnetic element like Mn^{2+} , known as diluted magnetic semiconductors (DMS's), typically possess either the cubic (zinc-blende) or the hexagonal (wurtzite) structure.¹ For instance, $\text{Cd}_{1-x}\text{Mn}_x\text{Te}$ and $\text{Zn}_{1-x}\text{Mn}_x\text{Te}$ have zinc-blende structure whereas $\text{Cd}_{1-x}\text{Mn}_x\text{Se}$ and $\text{Cd}_{1-x}\text{Mn}_x\text{S}$ occur with the wurtzite structure throughout the composition range accessible to bulk growth techniques. Recent successes in the growth of high-quality heterostructures of DMS's by molecular-beam epitaxy (MBE) (Refs. 2 and 3) provide opportunities to study physical phenomena not encountered in the bulk. For example, it has been demonstrated that $\text{Cd}_{1-x}\text{Mn}_x\text{Se}$ can be stabilized in the zinc-blende phase by growing epitaxial layers on (001) GaAs substrates using MBE.⁴

The vibrational spectra of semiconductor alloys illustrate many fundamental aspects of lattice vibrations and the physics of alloys. Raman scattering from phonons and various magnetic excitations in the DMS's with the zinc-blende structure has been investigated in great detail. The zone-center optical phonons in semiconducting alloys show a variety of behavior patterns: they exhibit a "one-mode," "two-mode," or "intermediate-mode" behavior depending on the vibrational characteristics of the end members.⁵ For example, optical phonons in $\text{Cd}_{1-x}\text{Mn}_x\text{Te}$ exhibit two-mode behavior⁶ while $\text{Zn}_{1-x}\text{Mn}_x\text{Te}$ and $\text{Zn}_{1-x}\text{Mn}_x\text{Se}$ in its zinc-blende-structure phase⁷ show an interesting intermediate-mode behavior pattern. In contrast, phonons in wurtzite-type DMS's have not been as extensively studied although the zone-center optical phonons in the wurtzite-structure semiconductors such as CdS (Refs. 8 and 9) and CdSe (Refs. 10 and 11) have been investigated thoroughly. This is the motivation of our study of Raman scattering from vibrational modes in $\text{Cd}_{1-x}\text{Mn}_x\text{Se}$ and $\text{Cd}_{1-x}\text{Mn}_x\text{S}$, both known to have wurtzite structures in

the composition range $0 < x < 0.50$ and $0 < x < 0.45$, respectively. Furthermore, the optical phonons in wurtzite structure $\text{Cd}_{1-x}\text{Mn}_x\text{Se}$ and the available information on the optical phonons in $\text{Cd}_{1-x}\text{Mn}_x\text{Se}$ epilayers with zinc-blende structure¹² enable us to examine the relationship between the properties of MBE-grown cubic and bulk-grown hexagonal structures.

We also note here that, in an external magnetic field, the Raman-electron-paramagnetic resonance (Raman-EPR) (Ref. 13) of Mn^{2+} and the spin-flip Raman scattering from donors¹⁴ have been reported for both $\text{Cd}_{1-x}\text{Mn}_x\text{Se}$ and $\text{Cd}_{1-x}\text{Mn}_x\text{S}$. In the present study, we have observed the Raman-EPR of Mn^{2+} in association with LO photons.

II. EXPERIMENT

The $\text{Cd}_{1-x}\text{Mn}_x\text{Se}$ samples with $x \leq 0.45$ and $\text{Cd}_{1-x}\text{Mn}_x\text{S}$ samples with $x \leq 0.125$ used in this work were single crystals grown with a modified Bridgman technique, the compositions being determined by electron microprobe measurements. All the samples were oriented using Laue diffraction and cut in the form of parallelepipeds and optically polished with a pair of faces normal to the c axis. Experiments were performed with either a variable temperature optical cryostat or a similar cryostat with a superconducting solenoid providing magnetic fields up to 60 kG. Raman spectra were excited using a variety of laser wavelengths provided by a Kr^+ , a He-Ne, and an Ar^+ laser. A computer-controlled double or triple monochromator and a standard photon counting system were used to analyze the scattered radiation.

III. RESULTS AND DISCUSSIONS

Crystals with the wurtzite structure are uniaxial and belong to the space group C_{6v}^4 ($P6_3mc$) with two formula units per primitive cell. The zone center optical phonons consist of $A_1 + 2B_1 + E_1 + 2E_2$ modes. Among these, A_1 and E_1 modes are both infrared and Raman active, E_2 modes are only Raman active, and B_1 modes are "silent"

TABLE I. Selection rules for wurtzite crystals (C_{6v}^4).

q	Geometry	Parallel (HH) polarization*	Crossed (VH) polarization*
$q \parallel \hat{c}$	Back scattering	A_1 (LO), E_2	E_2
$q \perp \hat{c}$	Back scattering	A_1 (TO), E_2	E_1 (TO)
	90° scatt.	E_2	E_1 (TO), E_1 (LO)

* H and V denote horizontal and vertical directions, the scattering plane being horizontal.

modes, i.e., inactive in both Raman scattering and infrared absorption. The A_1 and E_1 modes are polar modes and, thus, are polarized along and perpendicular to the optic axis (\hat{c}), respectively. Hence, for the phonon propagating with the wave vector q perpendicular to \hat{c} , the E_1 phonon splits into longitudinal (LO) and transverse (TO) modes due to the long-range polarization field, whereas the A_1 phonon remains as A_1 (TO). On the other hand, for $q \parallel \hat{c}$, only the A_1 (TO) phonon changes to A_1 (LO) due to the associated long-range polarization field, and the E_1 phonon remains doubly degenerate at the E_1 (TO) position. In uniaxial crystals, both LO-TO splitting and the crystal anisotropy due to the short-range interatomic forces have thus to be considered for the polar modes. It is known that in crystals with wurtzite structure, the LO-TO splitting dominates crystal anisotropy, and consequently, in a crystal with an arbitrary orientation, one observes LO and TO modes of mixed symmetry.⁸ Phonons of different symmetry can be identified from the polarization characteristics of their Raman lines deduced from the polarizability tensors.¹⁵ Based on polarizability tensors, selection rules summarized in Table I can be deduced; with the configurations specified, the A_1 , E_1 , and E_2 modes can be completely separated.

$Cd_{1-x}Mn_xSe$

Figure 1 shows the Raman spectra associated with the optical phonons in $Cd_{1-x}Mn_xSe$ ($x=0.20$) excited with the 6764-Å line of the Kr^+ laser, and recorded at the temperature $T=5$ K. The Raman-active phonons appear in one or more of the three different scattering configurations employed: the polarization geometry and the allowed phonon symmetries are indicated in Fig. 1. The low-frequency E_2 mode was not observed, presumably because of the decrease in the Bose population factor n_q , the intensity being proportional to $n_q + 1$. As can be seen in Fig. 1, in the mixed crystal new peaks appear at frequencies higher than those of the optical phonons of CdSe; they are assigned to "MnSe-like" phonons, evolving from the impurity mode of Mn^{2+} in CdSe for $x \rightarrow 0$. The frequency variation of optical phonons as a function of the Mn concentration is shown in Fig. 2. As in $Cd_{1-x}Mn_xTe$, the zone-center optical phonons in $Cd_{1-x}Mn_xSe$ also exhibit a two-mode behavior with "CdSe-like" and "MnSe-like" phonons corresponding to each of the A_1 and E_1 modes of pure CdSe. As x increases from 0 to 1, the Mn^{2+} local mode in CdSe (CdSe:Mn) evolves into MnSe-like LO and TO modes and finally becomes A_1 (LO), A_1 (TO), E_1 (TO), and E_1 (LO)

modes of the hypothetical MnSe with the wurtzite structure, whereas the LO and TO modes of CdSe become CdSe-like phonons of the mixed crystal and finally merge into a gap mode of Cd in wurtzite-structure MnSe (MnSe:Cd). As expected, the A_1 and E_1 splitting due to the crystal anisotropy is negligible compared to the LO-TO splitting.

Zone-center optical phonons in mixed crystals can be described in terms of a simple model called "random-element-isodisplacement" (REI), proposed by Chen, Shockley, and Pearson¹⁶ and modified subsequently by a number of authors.^{5,6,17} The fundamental assumptions of the REI model are (1) the two types of cations (anions) are randomly distributed on the cation (anion) sublattices, (2) each ion experiences the force produced by a statistical average of the interactions with its neighbors, and (3) in the long-wavelength limit the cations (anions) of like species vibrate as a rigid unit with the same phase and amplitude. In a modified model, a local field treat-

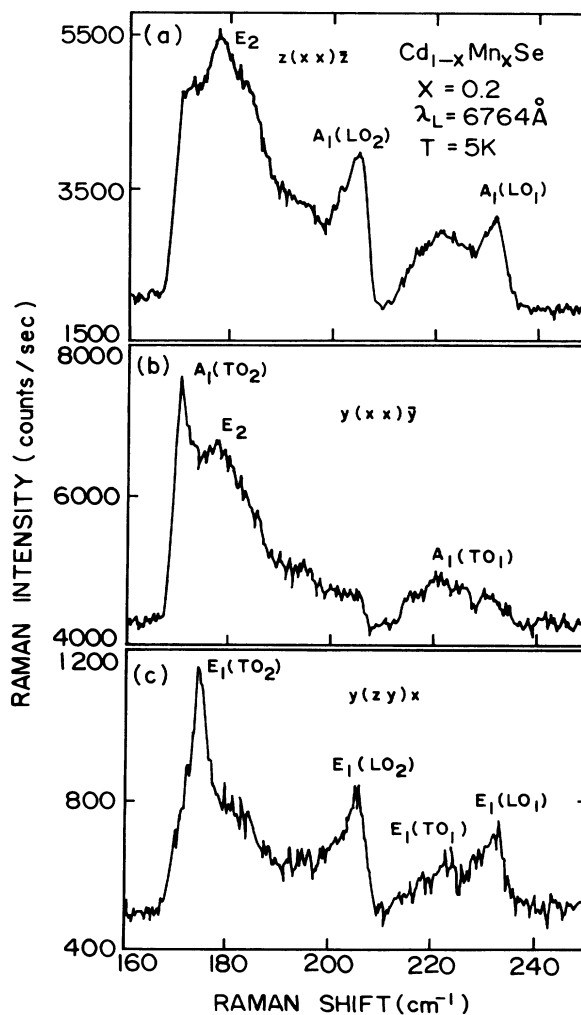


FIG. 1. Raman spectra of $Cd_{1-x}Mn_xSe$, $x=0.20$. Spectra obtained with the laser excitation having wavelength $\lambda_L=6764$ Å at $T=5$ K. Scattering configurations are (a) $z(xx)z$, (b) $y(xx)y$, and (c) $y(zy)x$. Here x , y , and z are mutually orthogonal with $\hat{z} \parallel \hat{c}$ and $\hat{x} \perp \sigma_v$, the vertical reflection plane in the wurtzite structure.

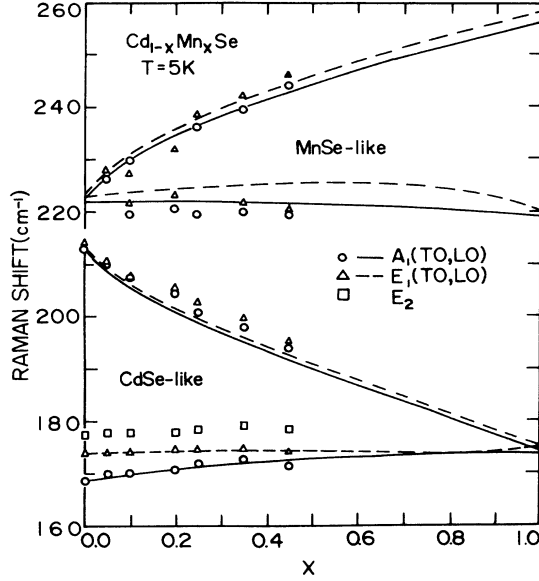


FIG. 2. Frequencies of zone-center optical phonons as a function of x in $\text{Cd}_{1-x}\text{Mn}_x\text{Se}$ at $T=5$ K. The curves were generated using MREI model described in Ref. 6.

ment has been incorporated. In this paper, we follow the modified random-element-isodisplacement. (MREI) model developed by Genzel, Martin, and Perry⁵ and used by Peterson *et al.*⁶ with the contributions of the local electric fields appropriate for a wurtzite structure.

Equations (1)–(4) of Ref. 6 as applied to $\text{Cd}_{1-x}\text{Mn}_x\text{Se}$, i.e., to a wurtzite-structure DMS, the local electric field at the site of vibrating ion, \mathbf{E}_{loc} , is given by¹⁸

$$\mathbf{E}_{\text{loc}} = \mathbf{E} + \frac{4\pi}{3} \mathbf{P} + \sum_{\text{sphere}} \mathbf{E}_d, \quad (1)$$

where \mathbf{E} is the macroscopic field, $(4\pi/3)\mathbf{P}$ is the contribution to the field from the surface polarization of the Lorentz sphere centered on that ion, and $\sum_{\text{sphere}} \mathbf{E}_d$ is the field due to all the point dipoles within that sphere. For a lattice having cubic symmetry, the last term vanishes for all modes of vibration. In wurtzite-structure crystals, the contribution from the last term is very small. Following Verleur and Barker,¹⁸ the \mathbf{E}_{loc} in $\text{Cd}_{1-x}\text{Mn}_x\text{Se}$ is given by

$$\mathbf{E}_{\text{loc}} = \mathbf{E} + \left[\frac{4\pi}{3} + C_i \right] \mathbf{P}, \quad i=1,2, \quad (2)$$

where C_i is a constant and the subscripts 1 and 2 represent its value for \mathbf{P} parallel or perpendicular to \hat{z} , respectively. The corrections to the Lorentz field, represented by C_i , have been calculated by Verleur and Barker¹⁸ for an ideal wurtzite structure: They are 0.2 for the mode polarized along the c axis and -0.1 for that polarized perpendicular to it.

The relationship between \mathbf{E}_{loc} and the electric polarization \mathbf{P} is

$$\mathbf{E}_{\text{loc}} = \left[\frac{4\pi}{3} + C_i \right] \mathbf{P}$$

for transverse modes and

$$\mathbf{E}_{\text{loc}} = - \left[\frac{8\pi}{3} - C_i \right] \mathbf{P}$$

for longitudinal modes. The force constants can be approximated by a function linear in x ,

$$f_i(x) = F_i \left[1 + \theta_i \frac{d_c - d(x)}{d_c} \right], \quad (3)$$

where d_c and d are the mean cation-cation distances of the alloys AC and $AB_{1-x}C_x$, respectively, and F_i and θ_i are constants.

The microscopic parameters in Eqs. (1)–(4) of Ref. 6, can be related to macroscopic parameters according to the Born-Huang procedure.¹⁹ For $x=0$,

$$\left[\frac{4\pi}{3} + C_i \right] \left[\frac{a_A + a_B}{v_b} \right] = \frac{\epsilon_{\infty b} - 1}{\epsilon_{\infty b} + \gamma}, \quad (4)$$

$$\frac{F_b}{\mu_B} \left[1 + \theta \frac{d_c - d_b}{d_c} \right] = \frac{\epsilon_{0b} + \gamma}{\epsilon_{\infty b} + \gamma} \omega_{\text{TO}b}^2. \quad (5)$$

$$\left[\frac{4\pi}{3} + C_i \right] \frac{e_b^2}{\mu_b v_b} = \frac{(\gamma + 1)(\epsilon_{0b} - \epsilon_{\infty b})}{(\epsilon_{\infty b} + \gamma)^2} \omega_{\text{TO}b}^2, \quad (6)$$

and for $x=1$,

$$\left[\frac{4\pi}{3} + C_i \right] \left[\frac{a_A + a_C}{v_c} \right] = \frac{\epsilon_{\infty c} - 1}{\epsilon_{\infty c} + \gamma}, \quad (4')$$

$$\frac{F_b}{\mu_B} = \frac{\epsilon_{0c} + \gamma}{\epsilon_{\infty c} + \gamma} \omega_{\text{TO}c}^2, \quad (5')$$

$$\left[\frac{4\pi}{3} + C_i \right] \frac{e_c^2}{\mu_c v_c} = \frac{(\gamma + 1)(\epsilon_{0c} - \epsilon_{\infty c})}{(\epsilon_{\infty c} + \gamma)^2} \omega_{\text{TO}c}^2. \quad (6')$$

Here

$$\gamma = \left[\frac{8\pi}{3} - C_i \right] / \left[\frac{4\pi}{3} + C_i \right],$$

μ_b and μ_c are the reduced masses, a 's are electronic polarizabilities of each ion, and v_b and v_c are the volume of the primitive cell; subscripts b and c refer to the alloys AB and AC . ϵ_{0b} , ϵ_{0c} , $\epsilon_{\infty b}$, and $\epsilon_{\infty c}$ are the static and high-frequency dielectric constants of the crystal AB and AC , and $\omega_{\text{TO}b}$ and $\omega_{\text{TO}c}$ are corresponding zone-center TO phonon frequencies. Here $A \equiv \text{Se}$, $B \equiv \text{Cd}$, and $C \equiv \text{Mn}$.

The frequencies of vibrational modes calculated using the MREI model are shown in Fig. 2. In this model, the frequencies of phonons in MnSe were assumed to be those of the hypothetical cubic MnSe obtained from the $x \rightarrow 1$ extrapolation of optical phonon frequencies in $\text{Zn}_{1-x}\text{Mn}_x\text{Se}$.⁷ The second-neighbor force constant F_s for each mode has been determined from the best fit to the experimental values of TO modes; they are $F_s = 0.507 F_b$ for A_1 modes and $F_s = 0.500 F_b$ for E_1 modes.²⁰ C_1 and C_2 are assumed to be 0.2 and -0.1 for the whole composition range. The parameters used to determine the frequencies of the vibrational modes and the resultant force constants are given in Table II. It should be noted

TABLE II. Parameters used in the MREI model for $\text{Cd}_{1-x}\text{Mn}_x\text{Se}$.

A_1 (cm ⁻²)		E_1 (cm ⁻²)	
CdSe	$\omega_{\text{TO}}=169$	CdSe	$\omega_{\text{TO}}=174$
	$\omega_{\text{LO}}=213$		$\omega_{\text{LO}}=214$
	ω_I (Mn)=222		ω_I (Mn)=223
	$\epsilon_0=9.91^{\text{a}}$		$\epsilon_0=9.15^{\text{a}}$
MnSe	$\omega_{\text{TO}}=219$	MnSe	$\omega_{\text{TO}}=220$
	$\omega_{\text{LO}}=256$		$\omega_{\text{LO}}=258$
	ω_I (Cd)=174		ω_I (Cd)=175
$d_c=4.296-0.123x$			
Force constants [10 ⁶ a.m.u. (cm ⁻¹) ²]			
A_1		E_1	
F_b^{b}	2.26		2.28
F_c^{b}	2.03		2.04
F_s^{b}	1.14		1.16

^aDielectric constants at $T = 100$ K. See Ref. 21.

^bSubscripts b , c , and s refer to Cd-Se, Mn-Se, and Cd-Mn, respectively.

that the magnitude of the second-neighbor force constants obtained are about half of the nearest-neighbor constants and hence this model does not give real frequencies for the vibrational modes if the second-neighbor force constants are neglected. This may indicate the limitation of the MREI model. As pointed out earlier, the anisotropic crystal-field splitting of vibrational modes is very small, as can be seen in Fig. 2. The small anisotropy has been taken into account in terms of direction-dependent force constants and charges which are related to anisotropic dielectric constants. In addition, small corrections to the local electric field C_i are also included. As illustrated in Fig. 2, the MREI model gives a reasonable description of the two-mode behavior of this alloy. It is also interesting to note that E_2 modes, as well as all TO modes, do not show a noticeable dependence on x . We believe this is due to the absence of polarization fields associated with these modes. The large frequency variation observed in LO modes can be attributed to the long-range polarization field associated with them.

In Fig. 3 we show the Raman spectrum of $\text{Cd}_{1-x}\text{Mn}_x\text{Se}$ ($x = 0.1$) with $H = 60$ kG; the intensities of Raman peaks are resonantly enhanced by the close match between the scattered photon energy with that of donor-acceptor recombination. A peak labeled PM is the Raman line associated with the spin-flip transition between the adjacent levels of the Zeeman multiplet of Mn^{2+} , i.e., it is due to the Raman EPR of Mn^{2+} (Ref. 13); this Raman shift is characterized by a g factor of 2, expected for Mn^{2+} . In the optical phonon region, the CdSe-like and MnSe-like E_1 (LO), as well as their combination with PM lines, are observed. Since the Raman mechanism of the PM line involves interband transitions,¹³ and the electrons and holes interact strongly with LO phonons via the Fröhlich interaction, LO phonons can be created or annihilated during the $\Delta M_s = \pm 1$ transitions in the Zeeman multiplet of Mn^{2+} . When the scattering

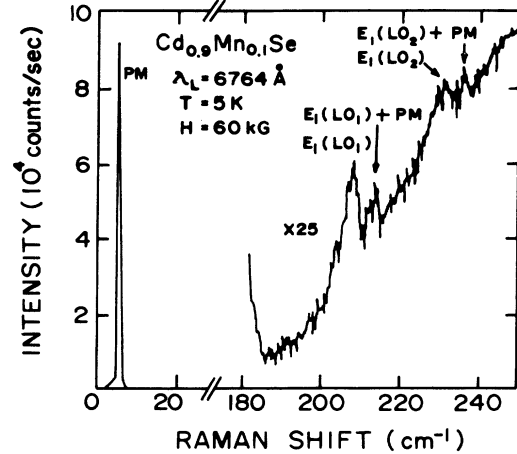


FIG. 3. Raman spectrum of $\text{Cd}_{1-x}\text{Mn}_x\text{Se}$, $x = 0.10$, at $T = 5$ K and $H = 60$ kG.

configuration is changed to $\mathbf{q} \parallel \hat{c}$, the A (LO) and its combination with the PM line, i.e., A_1 (LO) \pm PM, are observed.

$\text{Cd}_{1-x}\text{Mn}_x\text{S}$

In Fig. 4, Raman spectra of optical phonons in $\text{Cd}_{1-x}\text{Mn}_x\text{S}$ ($x = 0.02$) are shown for three different configurations. New modes originating from the impurity modes of Mn in CdS appear between LO and TO frequencies.

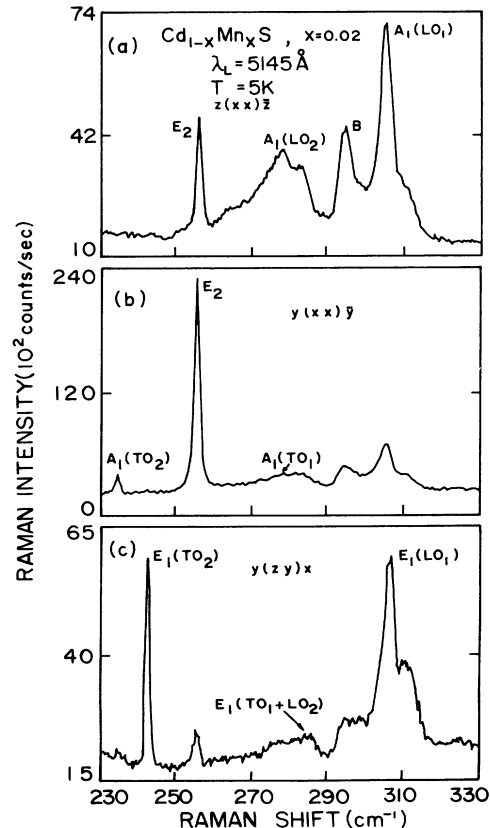


FIG. 4. Raman spectra of $\text{Cd}_{1-x}\text{Mn}_x\text{S}$, $x = 0.02$, excited with $\lambda_L = 5145$ Å at $T = 5$ K. (a) $z(xx)z$, (b) $y(xx)y$, and (c) $y(zy)x$.

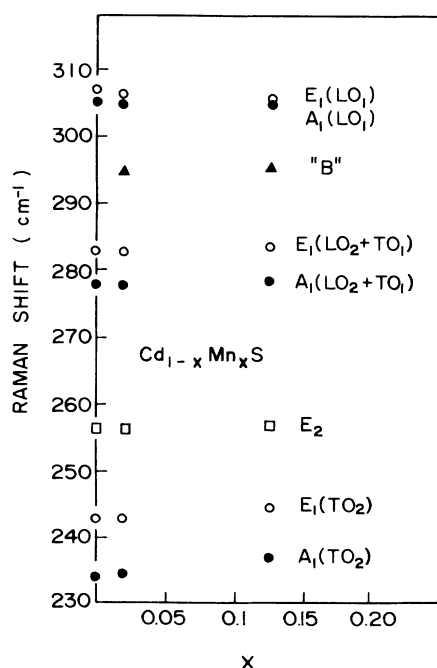


FIG. 5. Frequencies of zone-center optical phonons as a function of x in $\text{Cd}_{1-x}\text{Mn}_x\text{S}$ at $T = 5$ K.

quencies of CdS , suggesting that $\text{Cd}_{1-x}\text{Mn}_x\text{S}$ exhibits an intermediate-mode behavior. Frequencies of the modes having A_1 or E_1 characteristics agree well with those of the resonant mode of a Mn impurity in CdS observed in the infrared absorption measurement.²² The frequencies of optical phonons in $\text{Cd}_{1-x}\text{Mn}_x\text{S}$ at $T = 5$ K are shown in Fig. 5 for $x = 0.02$ and $x = 0.125$. The LO-TO modes originating from the impurity modes are not well resolved for samples with the low Mn^{2+} concentration studied in the present investigation.

In addition, as can be seen in Fig. 4(a), a distinct peak

having A_1 symmetry is observed and labeled B . The frequency of B does not show a noticeable dependence on x while its intensity increases with x . This mode can be identified with the "breathing mode"²³ of nearest neighbor S atoms Mn^{2+} . It is interesting to note that a similar mode was observed with a Raman shift close to that of the breathing mode in $\text{Zn}_{1-x}\text{Mn}_x\text{S}$ (Ref. 24), suggesting that the Mn-S force constant is not significantly different in the two systems.

IV. CONCLUSION

The present study shows that vibrational modes in $\text{Cd}_{1-x}\text{Mn}_x\text{Se}$ display a two-mode behavior, as in $\text{Cd}_{1-x}\text{Mn}_x\text{Te}$, as a function of x . The small anisotropy due to the crystal field in the wurtzite structure can be attributed to direction-dependent force constants, charges, and the local electric field. The second-neighbor force constant deduced from the best fit of the MREI model to the experimental frequencies of TO modes is significantly large, whereas the local electric field correction is negligible. An extrapolation of the vibrational modes to $x = 1$ provides an insight into many of the physical characteristics of the hypothetical wurtzite-structure MnSe . Similar information can be obtained by studying the vibrational modes in $\text{Cd}_{1-x}\text{Mn}_x\text{S}$ as a function of x ; although such a study has yet to be completed, the data appear to suggest that the vibrational modes in $\text{Cd}_{1-x}\text{Mn}_x\text{S}$ exhibit a behavior intermediate between the one-mode and two-mode behavior.

ACKNOWLEDGMENTS

The investigation reported in the present paper received support from the National Science Foundation, Grant No. DR-86-16787, at Purdue University. E.S. acknowledges support from Korea Science and Engineering Foundation.

*Present address: Semiconductor Physics Research Center and Department of Physics, Jeonbuk National University, Jeonju 560-756, Republic of Korea.

†Present address: Material Science Laboratory, Reactor Research Center, Kalpakkam 603 102, Tamilnadu, India.

¹J. K. Furdyna, *J. Appl. Phys.* **64**, R29 (1988).

²L. A. Kolodziejski, T. C. Bonsett, R. L. Gunshor, S. Datta, R. B. Bylsma, W. M. Becker, and N. Otsuka, *Appl. Phys. Lett.* **45**, 92 (1984).

³R. N. Bicknell, N. C. Giles, and J. F. Schetzina, *Appl. Phys. Lett.* **50**, 691 (1987).

⁴N. Samarth, H. Luo, J. K. Furdyna, S. B. Quadri, Y. R. Lee, A. K. Ramdas, and N. Otsuka, *Appl. Phys. Lett.* **54**, 2680 (1989).

⁵L. Genzel, T. P. Martin, and C. H. Perry, *Phys. Status Solidi B* **62**, 83 (1974).

⁶D. L. Peterson, A. Petrou, W. Girit, A. K. Ramdas, and S. Rodriguez, *Phys. Rev. B* **33**, 1160 (1986).

⁷A. K. Arora, E.-K. Suh, U. Debska, and A. K. Ramdas, *Phys. Rev. B* **37**, 2927 (1988).

⁸See, for example, C. A. Arguello, P. L. Rousseau, and S. P. S. Porto, *Phys. Rev.* **181**, 1351 (1969).

⁹R. J. Briggs and A. K. Ramdas, *Phys. Rev. B* **13**, 5518 (1976).

¹⁰V. G. Plotnichenko, Yu. A. Mityagin, and L. K. Vodop'yanov, *Fiz. Tverd. Tela (Leningrad)* **19**, 2706 (1977) [*Sov. Phys. Solid State* **19**, 1584 (1977)].

¹¹A. K. Arora and A. K. Ramdas, *Phys. Rev. B* **35**, 4345 (1987).

¹²R. G. Alonso, E.-K. Suh, A. K. Ramdas, N. Samarth, H. Luo, and J. K. Furdyna, *Phys. Rev. B* **40**, 3720 (1989).

¹³A. Petrou, D. L. Peterson, S. Venugopalan, R. R. Galazka, A. K. Ramdas, and S. Rodriguez, *Phys. Rev. B* **27**, 3471 (1983).

¹⁴D. L. Peterson, D. U. Bartholomew, U. Debska, A. K. Ramdas, and S. Rodriguez, *Phys. Rev. B* **32**, 323 (1985).

¹⁵See, for example, M. Cardona, in *Light Scattering in Solids II*, edited by M. Cardona and G. Güntherodt, Topics in Applied Physics Vol. 50 (Springer-Verlag, Berlin, 1982), pp. 46–49.

¹⁶Y. S. Chen, W. Shockley, and G. L. Pearson, *Phys. Rev.* **151**, 648 (1966).

¹⁷I. F. Chang and S. S. Mitra, *Phys. Rev.* **172**, 924 (1968).

¹⁸H. W. Verleur and A. S. Barker, Jr., *Phys. Rev.* **155**, 750 (1967).

¹⁹M. Born and K. Huang, *Dynamical Theory of Crystal Lattices* (Oxford University Press, London, 1968).

²⁰It turned out that $F_s = (0.507 \pm 0.001)F_b$ for the A_1 modes and $F_s = (0.500 \pm 0.001)F_b$ for the E_1 modes give the smallest de-

- viation of calculated values from experimental values for TO modes estimated for seven different x values.
- ²¹R. Geick, C. H. Perry, and S. S. Mitra, J. Appl. Phys. **37**, 1994 (1966).
- ²²M. A. Nusimovici, M. Balkanski, and J. L. Birman, Phys. Rev. B **1**, 603 (1970).
- ²³S. Venugopalan, A. Petrou, R. R. Galaska, A. K. Ramdas, and S. Rodriguez, Phys. Rev. B **25**, 2681 (1982).
- ²⁴A. Anastassiadou, E. Liarokapis, and E. Anastassakis, Phys. Scr. **38**, 444 (1988).